Journal of Nano- and Electronic Physics
Vol. **16** No 6, 06029(6pp) (2024)

Журнал нано- та електронної фізики
Том **16** № 6, 06029(6cc) (2024)

OPEN ACCESS

REGULAR ARTICLE

Photonic Crystal Fibers with Triangular and Kagome Structures for Fiber Optic Gyroscopes

E.N. Odarenko, O.S. Hnatenko*

Kharkiv National University of Radio Electronics, 61166 Kharkiv, Ukraine

(Received 22 August 2024; revised manuscript received 15 December 2024; published online 23 December 2024)

The article investigates photonic crystal fibers (PCFs) with triangular and kagome structures for use in fiber optic gyroscopes (FOGs). The advantages of PCFs in enhancing FOG performance are substantiated, highlighting their unique features, such as high sensitivity, low optical losses, and resistance to temperature fluctuations. Mechanisms of energy localization through photonic bandgaps and single-mode operation are discussed to improve measurement accuracy. Numerical calculations of dispersion characteristics and eigenmodes of PCFs were performed using the plane wave expansion method in the MIT Photonic Bands software. The modal properties of various PCF designs were analyzed, focusing on the impact of hollow core diameter on spectral characteristics. It is demonstrated that the optimal ratio of geometric parameters ensures effective energy localization in the hollow core and minimizes losses.Special attention is given to PCFs with kagome lattices, which show potential for reducing energy losses due to the spatial distribution of the electromagnetic field. Conclusions are drawn about the application of PCFs in gyroscopes for aviation and defense navigation systems. The findings open new possibilities for developing high-precision equipment capable of operating under extreme conditions.

Keywords: Photonic crystal, Optical fiber, Gyroscope, Dispersion characteristics, Bandgap.

DOI: 10.21272/jnep.16(6).06029 PACS numbers: 42.55.Tv, 42.81. – i, 42.81.Pa

1. INTRODUCTION

Fiber optic gyroscopes (FOGs) use the Sagnac effect [1], where light waves traveling in opposite directions in a closed loop accumulate a phase shift proportional to the angular velocity of the system's rotation. Photonic crystal fibers (PCFs) offer unique properties that enhance FOG performance [3-4]. Their periodic structure creates photonic band gaps for efficient light localization, while birefringence reduces noise and improves measurement accuracy. PCFs are also resistant to mechanical impacts and temperature fluctuations, ensuring reliable operation in extreme conditions. Photonic crystal structures are widely used to create various functional devices: waveguides, resonators, filters, etc. [5-6]. Photonic crystal waveguides of various dimensions are basic components of many modern optoelectronic systems [7-9]. Microstructured optical waveguides are a type of such waveguides and can be identified as photonic crystal fiber waveguides [10]. PCFs are actively researched for applications in optical sensors and gyroscopes. Their ability to guide light through a hollow core allows precise rotation angle measurement, making them ideal for aerospace and defense navigation systems. Their low losses, dual beam splitting, and high sensitivity improve the signal-to-noise ratio and reduce crosstalk, opening new possibilities for precise measurement systems.

PCFs with hollow cores localize energy through the photonic bandgap mechanism, allowing single-mode waveguides even for large hollow core cross-sections.

Thus, the main operational characteristics of photonic crystal fibers are determined by the electrodynamic properties of the periodic cladding of the waveguide channel, which essentially represents a two-dimensional photonic crystal. This crystal is formed by a hexagonal lattice of hollow holes in silicon glass with a dielectric permittivity of ε = 2.1. The thickness of the walls between the holes is much smaller than the lattice period, thereby forming an environment with an effective dielectric permittivity close to one. This waveguide cross-sectional configuration significantly reduces losses that occur during the propagation of electromagnetic waves in the dielectric medium.

2. CALCULATION OF THE EIGENMODES OF PHOTONIC CRYSTAL FIBER WAVEGUIDES

2.1 Dispersion Characteristics of Photonic Crystal Fiber with a Cladding in the Form of a Triangular Lattice of Hollow Holes

The dispersion characteristics of the photonic crystal forming the cladding of the fiber waveguide serve as the foundation for determining the eigenmode characteristics of the photonic crystal fiber. Figure 3.1 presents a schematic representation of a two-dimensional photonic crystal, consisting of periodically arranged hollow cylindrical holes within a dielectric (silicon glass) array, along with the corresponding oblique coordinate system. The period of the structure

* Corresponding email: oleksandr.hnatenko@nure.ua

Cite this article as: E.N. Odarenko et al., *J. Nano- Electron. Phys.* 16 No 6, 06029 (2024) https://doi.org/10.21272/jnep.16(6).06029

is defined as the distance between the centers of any two nearest cylinders. The radius of the cylinders, normalized to the period of the structure L, is $r/L = 0.48$. This configuration is commonly used for modeling photonic crystal fiber waveguides. For the calculations of the dispersion characteristics, the specialized software package MIT Photonic Bands, which is freely distributed and open-source [11], was used. This software is widely applied for the study of photonic crystal structures and utilizes the plane wave expansion method, commonly used to determine the eigenmodes of various periodic systems of different dimensions. The periodic structure is formed in the standard way by creating a unit cell and applying the property of translational invariance.

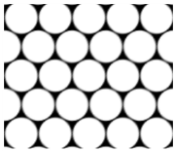

Fig. 1 – Diagram of the Photonic Crystal

The dispersion properties of the basic configurations of photonic crystals are well-studied [12]. It is known that under certain conditions, the structure shown in Figure 1 has photonic band gaps for two polarization states (*TE* and *TM*). In particular, the widest band gap is realized for *TE* polarization, where the magnetic field vector is directed along the O_z axis.

The results of the dispersion diagram calculations for a two-dimensional photonic crystal with a triangular lattice of hollow cylinders are presented in Figure 2 for *TE* polarization.

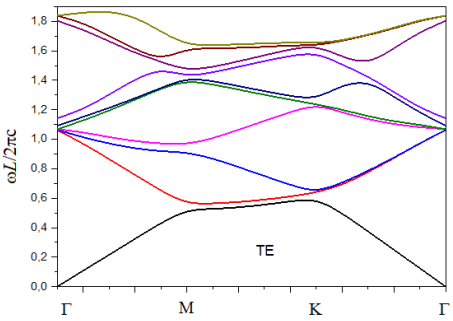

Fig. 2 – Dispersion diagrams of the photonic crystal for *TE* polarization states

Along the abscissa axis, the values of the Bloch wavevector are plotted within the unreduced first Brillouin zone. Points of high symmetry within this zone are marked by letters. Along the ordinate axis, the normalized frequency is plotted, which is essentially the ratio of the structure's period to the wavelength of the radiation.

From Figure 2, it is evident that in this case, photonic band gaps are absent for this polarization. This result is due to the low dielectric contrast in the studied structure (2.1:1). It should be noted that the results presented in Figure 2 were obtained for the case where the longitudinal component of the wavevector is zero, i.e., $k_z = 0$. This means that the waves propagate only in the xy-plane. In a fiber waveguide, propagation occurs along the Oz coordinate axis ($k_z \neq 0$), i.e., perpendicular to the plane of the diagram. Therefore, to study the eigenmodes of the photonic crystal fiber waveguide, the dispersion characteristics of the photonic crystal must be considered for nonzero values of the longitudinal wavevector component (the propagation constant).

It is known that increasing the propagation constant leads to the appearance of photonic band gaps in the structure shown in Figure 1. The physical factors behind this phenomenon are typically explained by the conditions of the so-called scalar approximation when the value of k_z increases [11]. Under these conditions, the electrodynamic characteristics of the dielectric photonic crystal resemble those of a crystal made of metallic cylinders and exhibiting multiple photonic band gaps. Thus, starting from a certain value of the propagation constant, photonic band gaps should appear in the photonic crystal that forms the waveguide cladding. It is within these gaps that the localization of electromagnetic energy in the waveguide channel and the realization of the eigenmodes of the photonic crystal fiber waveguide can occur.

Figure 3 presents the results of dispersion characteristic calculations for nonzero values of the longitudinal wavevector component. Along the abscissa axis, the normalized propagation constant values are plotted. The dashed line represents the "light line," where points correspond to cases where the phase velocity of the waves equals the speed of light in a vacuum.

The light areas of the dispersion diagram in Figure 3 correspond to the forbidden zones of the photonic crystal. It can be seen that, starting from the value $k_zL/2\pi = 1.43$, a photonic band gap opens up, which gradually expands as the propagation constant increases. At the same time, there is only a limited range of $k_zL/2\pi$ values where this band gap lies above the light line, indicating the possibility of realizing eigenmodes of the structure that correspond to volume waves. The region of the diagram below the light line corresponds to surface wave modes, whose field exponentially decays in free space. Additionally, the energy of surface waves is concentrated on the surfaces of the dielectric elements of the structure, leading to additional losses. Therefore, surface wave modes are generally not used as operating modes in photonic crystal fiber waveguides.

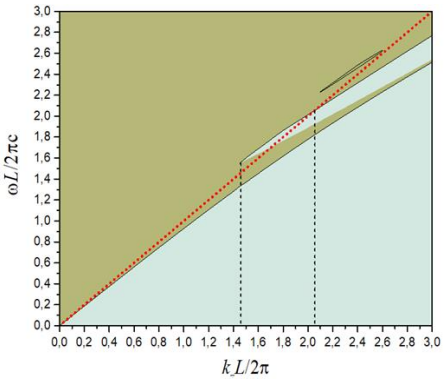

Fig. 3 – Dispersion diagram of the photonic crystal for the longitudinal component of the wavevector

Thus, the operating range of the photonic crystal fiber waveguide is limited. The vertical dashed lines in Figure 3 indicate the boundary values of the propagation constant.

The results of the dispersion diagram calculations for different values of the propagation constant are presented in Figure 4. The diagram in Figure 3.4a is calculated for a value of the parameter $k_zL/2\pi$ outside the operating range of the waveguide. Indeed, in this case, only the zero photonic band gap exists, in which the eigenmodes can only exist as surface wave modes.

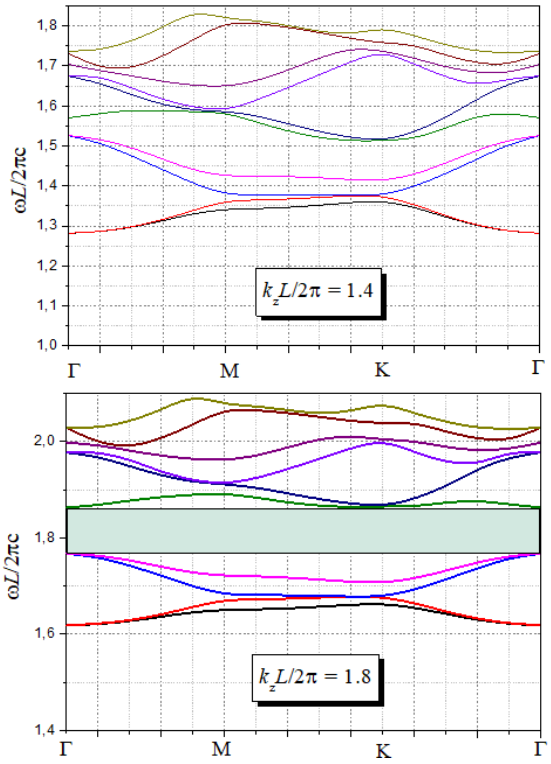

Fig. 4 – Dispersion diagrams of the photonic crystal for different values of the longitudinal wavevector

The diagram in Figure 4 is calculated within the operating range of propagation constant values. The horizontal band represents the photonic band gap, where the eigenmodes of the structure can exist both as surface and volume waves. This band gap opens as the propagation constant of the waveguide increases.

2.2 Eigenmode Characteristics of Photonic Crystal Fibers

An important characteristic of the eigenmodes of photonic crystal fiber waveguides is the distribution of the electromagnetic field across the cross-section of the structure. This distribution allows us to determine the mode structure of the waveguide and the energy losses due to its penetration into the cladding of the waveguide channel. A convenient way to visualize this is through the calculation of the spatial distribution of field intensity, which effectively represents an energetic characteristic. Therefore, numerical calculations were carried out for the energy of the electric field of the eigenmodes of the photonic crystal fiber waveguide.

Since the MIT Photonic Bands package is designed to determine the characteristics of eigenmodes for periodic structures only, it cannot be directly used for studying structures with defects in periodicity, such as photonic crystal waveguides and resonators. This problem is solved by using the supercell method, which restores the periodicity of the structure by creating a new cell with larger dimensions [14]. However, when applying this method, a larger number of dispersion curves must be calculated due to the increased number of eigenfrequencies in the supercell compared to a regular unit cell. Furthermore, in this case, only those eigenmodes of the built periodic structure are considered valid, which are characterized by the absence of electromagnetic coupling between neighboring periodicity defects.

Let us consider several variants of the fiber waveguide cross-section, differing in the radius of the hollow core. The first variant has a radius value normalized to the structure period of $R/L = 0.83$. Figure 5 shows the cross-section of the corresponding photonic crystal fiber.

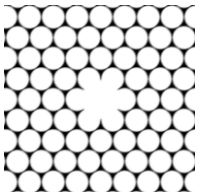

Fig. 5 – Diagram of the photonic crystal fiber

As seen in Figure 5, in this case, the configuration of the hollow waveguide channel cross-section ensures the absence of eigenmodes of the structure corresponding to surface waves [15-16]. This is confirmed by the results of calculations of the spatial distribution of the electric field intensity in the waveguide cross-section, as shown in Figure 6.

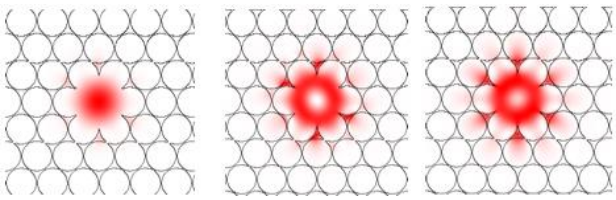

$\omega L/2\pi c = 1.7317$ $\omega L/2\pi c = 1.7668$ $\omega L/2\pi c = 1.7684$

Fig. 6 – Spatial distributions of the electric field intensity of the eigenmodes of the photonic crystal fiber waveguide

It is quite natural that the fundamental mode of the waveguide corresponds to the lowest frequency. In this mode, the most effective localization of energy occurs in the hollow core of the structure. It should be noted that the calculation results presented in Figure 6 were obtained for a fixed propagation constant value of $k_zL/2\pi = 1.7$. Therefore, all the spatial distributions of the electric field intensity correspond to the eigenmodes of the structure for bulk waves, since the corresponding eigenfrequencies are greater than 1.7. For higher modes, a more significant penetration of energy into the waveguide's cladding is observed, which increases the losses.

Figure 7 shows the cross-section diagram of a photonic crystal fiber waveguide with a normalized hollow core radius of $R/L = 1.5$. This configuration

supports the existence of eigenmodes on surface waves, which is determined by the structure of the boundary of the hollow waveguide channel.

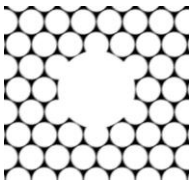

Fig. 7 – Cross-section diagram of a photonic crystal fiber waveguide

This conclusion is confirmed by the results of calculations of the spatial distributions of the electric field intensity for the eigenmodes of the structure, as shown in Figure 8. From Figure 8, it can be seen that in this case, nearly all the eigenmodes of the structure are hybrid, meaning they combine characteristics of both bulk and surface wave modes. Another interpretation of the obtained results is the overlap of the regions where the bulk and surface modes of the waveguide exist.

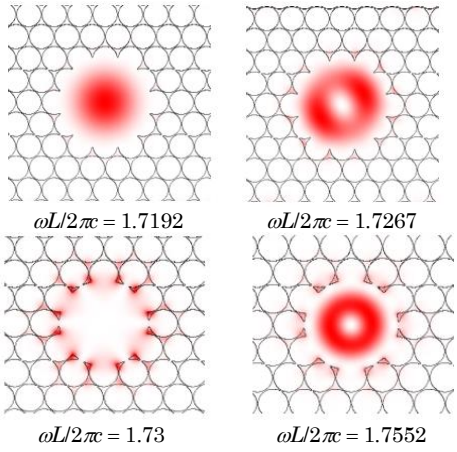

Fig. 8 – Spatial distributions of the electric field intensity for the eigenmodes of the photonic crystal fiber waveguide

A significant portion of the energy is concentrated in the dielectric, which leads to increased losses in the waveguide channel and, consequently, deteriorates the energy characteristics of the photonic crystal fiber waveguide. In Figure 9, the cross-section diagram of the waveguide with an increased hollow waveguide channel radius value of $R/L = 1.8$ is presented.

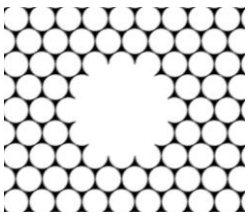

Fig. 9 – Cross-section diagram of the photonic crystal fiber waveguide

This cross-section configuration of the photonic crystal fiber waveguide also provides a fairly weak coupling between the bulk and surface modes, which allows for improved localization of electromagnetic energy in the hollow core [15]. However, unlike the waveguide with smaller core radii, in this case, the waveguide becomes significantly multimodal. As a result, the frequency range in which only the bulk wave modes can exist is reduced.

Figure 10 presents the results of the calculation of the spatial distribution of the electric field intensity for the waveguide modes corresponding to bulk waves.

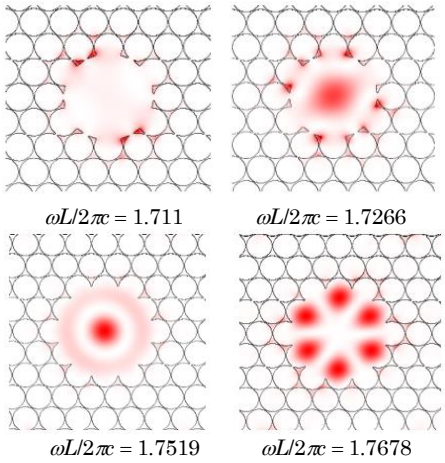

Fig. 10 – Spatial distribution of the electric field intensity for the eigenmodes of the photonic crystal fiber waveguide

It is evident that both axially symmetric and asymmetric modes can be realized. It is important to note the increase in the efficiency of field energy localization for the fundamental mode compared to configurations with a smaller hollow core radius. This is a fully expected result, as it is known that energy outside the waveguide channel decreases as $1/R^3$ when the core radius R increases [15-16].

The calculation results show that for higher modes, the energy outside the waveguide channel increases compared to the fundamental mode. Therefore, the working range of the waveguide is typically the single-mode range, where energy losses are minimized.

2.3 Characteristics of a Photonic Crystal Fiber with a Kagome Lattice Cladding

The calculation of the dispersion characteristics of a photonic crystal fiber waveguide based on a kagome lattice was performed, as in the previous case, using the supercell method. The result of constructing the structure for dispersion characteristic calculations using the supercell method is presented in Figure 11. In this case, the hollow core of the fiber waveguide has the shape of a regular hexagon [17-19].

From Figure 11, it can be observed that the nearest neighboring waveguide cores are separated by four periods of the structure. Additional calculations have shown that such a distance is sufficient to ensure electromagnetic isolation between these cores in cases where guided modes of the structure localize energy in the central part of the supercell. It should be noted that increasing the distance between the hollow cores leads to an increase in the size of the supercell and a corresponding significant rise in the computational resources required.

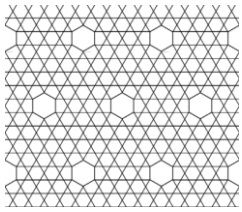

Fig. 11 – Schematic model of a photonic crystal fiber waveguide based on a kagome lattice

Figure 12 presents the results of the calculations of the dispersion characteristics of the fiber waveguide. The dependencies of the normalized frequency on the normalized longitudinal wave number were calculated by considering 500 dispersion curves. This is due to the large size of the supercell and the corresponding increase in the multiple eigenfrequencies of the structure. The dashed inclined line represents the light line for a vacuum.

In Figure 12, a photonic bandgap can be observed, which emerges with an increase in the longitudinal wave number (as shown in Figure 10). This bandgap is located below the light line in the region where guided modes on surface waves are realized. At the same time, in the region where guided modes on bulk waves exist, near the light line, no bandgaps are present. It is this region of the dispersion diagram that contains the operational modes of the waveguide.

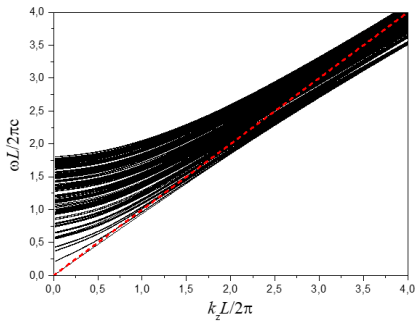

Fig. 12 – Dispersion characteristic of a photonic crystal waveguide based on a kagome lattice

The calculation of field characteristics for the guided modes of a photonic crystal fiber waveguide based on a kagome lattice was performed, as in the previous case, for the intensity of the electric field in the waveguide cross-section. The selected distributions of intensity were those for which electromagnetic isolation between the centers of neighboring supercells is achieved. In this case, the calculation results correspond to the guided modes of the fiber waveguide.

Figure 13 shows the spatial distributions of the electric field intensity for the guided modes of the structure, which are located on the dispersion diagram below the light line. This follows from the normalized eigenfrequencies of these modes, as the calculation was conducted for a normalized propagation constant $k_zL/2\pi = 4$. Such a configuration of the guided modes indicates the surface nature of the electromagnetic field, as confirmed by Figure 13. It can be seen that the field energy is concentrated in the dielectric plates that form the kagome structure. As the distance from the dielectric increases into free space, the field undergoes exponential decay. The greatest practical interest lies not in the surface guided modes, but in the bulk guided modes of the kagome fiber waveguide, as in this case, the field energy propagates through free space with minimal losses.

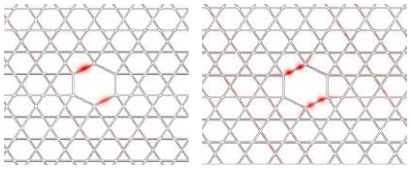

Fig. 13 – Spatial distributions of the electric field intensity for surface guided modes of the fiber waveguide

Figure 14 presents the results of the calculation of the spatial distribution of the electric field intensity in the projection onto the (x, y) plane for the fundamental and the first higher modes of the waveguide.

The fundamental mode is characterized by the absence of field variations in the cross-section of the structure and the highest degree of electromagnetic energy localization within the waveguide channel. The first higher mode has two intensity maxima of the electric field in the waveguide channel cross-section. Accordingly, a zero intensity value is realized at the center of the channel. Moreover, the effectiveness of electromagnetic energy localization in this case is lower compared to the fundamental mode. This is a natural result, as for higher modes, the intensity maxima occur closer to the boundaries of the waveguide channel, leading to an increase in the field amplitude at these boundaries. Consequently, energy losses of the mode increase within the core due to its passage into the waveguide cladding.

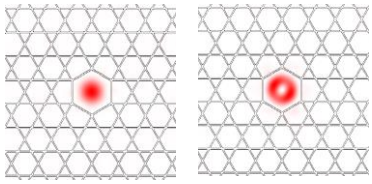

Fig. 14 – Spatial distributions of the electric field intensity for the guided modes of the fiber waveguide on bulk waves

Figure 15 shows the spatial distributions of the electric field intensity for two higher modes of the structure. One of these modes (on the left in the figure) has an almost axially symmetric spatial distribution of the field intensity within the waveguide channel. It should be noted that for this mode, a maximum field intensity is realized at the center of the channel, with the diameter of the cross-section of this maximum being significantly smaller than the width of the field spot for the fundamental mode (Figure 14). However, in this case, a much larger portion of the mode's field energy is located outside the waveguide channel, leading to increased losses.

CONCLUSION

The mathematical models for two configurations of photonic crystal fiber waveguides with hollow cores have been constructed. Numerical calculations of the

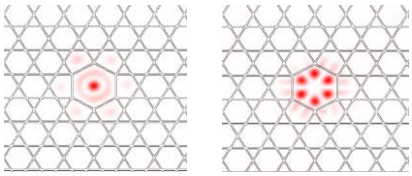

Fig. 15 – Spatial distributions of the electric field intensity for higher modes of the fiber waveguide on bulk waves

electrodynamic characteristics of the guided modes were performed using the plane wave expansion method, implemented in the MIT Photonic Bands software package, which is freely distributed and has open-source code. The obtained dispersion and field characteristics provide the opportunity to study the mode composition of different photonic crystal fiber waveguide configurations and their spectral properties.

The conducted research shows that proper integration of photonic crystal fibers into the design of fiber-optic gyroscopes (FOGs) can significantly improve their efficiency, as these fibers are capable of ensuring low optical losses and resistance to temperature fluctuations, which is crucial for the stable operation of gyroscopes. Taking into account all the technological aspects discussed in this section is necessary for the creation of high-precision and reliable FOGs capable of operating in various conditions. These results highlight the importance of technological and design improvements for the development of modern fiber-optic gyroscopes.

REFERENCES

1. Eric Udd, William B. Spillman Jr., *Fiber Optic Sensors: An Introduction for Engineers and Scientists, 2nd Ed.* (John Wiley & Sons, Inc.: 2011).
2. Yu.S. Kurskoy, O.S. Hnatenko, O.V. Afanasieva, *J. Nano-Electron. Phys.* **15** No 6, 06023 (2023).
3. Yu.P. Machekhin, Yu.S. Kurskoy, A.S. Gnatenko, *Telecommun. Radio Eng.* **77** No 18, 1631 (2018).
4. O.S. Hnatenko, Yu.P. Machekhin, V. Bilichenko, V. Zarytskyi, Y. Yaroslavskyy, J. Klimek, K. Mussabekov, B. Yeraliyeva, A. Ormanbekova, *Proc. SPIE* **12985**, *Optical Fibers and their Applications 2023*, 1298508 (2023).
5. Q. Gong, X. Hu, *Photonic Crystals. Principles and Applications* (Pan Stanford Publishing: 2013).
6. Y.C. Lin, S.H.Chou, W.J. Hsueh, *Sci. Rep.* **10**, 7040 (2020).
7. G.M. Katyba, K.I. Zaytsev, N.V. Chernomyrdin, I.A. Shikunova, G.A. Komandin, V.B. Anzin, S.P. Lebedev, I.E. Spektor, V.E. Karasik, S.O. Yurchenko, I.V. Reshetov, V.N. Kurlov, M. Skorobogatiy, *Adv. Opt. Mater.* **6** No 22, 1800573 (2018).
8. Y. Huang, X. Mao, D.C. Zhang, L. Cao, K. Cui, W. Zhang, J. Peng, *Chinese Opt. Lett.* **6** No 10, 704 (2008).
9. Ya.V. Sashkova, Ye.N. Odarenko, *Telecommun. Radio Eng.* **77** No 6, 489 (2018).
10. N.M. Litchinitser, S.C. Dunn, B. Usner, B.J. Eggleton, T.P. White, R.C. McPhedran, C.M. de Sterke, *Opt. Exp.* **11**, 1243 (2003).
11. S.G. Johnson, J.D. Joannopoulos, *Opt. Exp.* **8**, 173 (2001).
12. J.D. Joannopoulos, S.G. Johnson, J.N. Winn, R.D. Meade, *Photonic Crystals: Molding the Flow of Light, 2nd Ed.* (Princeton University Press: 2008).
13. K.K. Lee, A. Farjadpour, Y. Avniel, J.D. Joannopoulos, S.G. Johnson. *Proc. SPIE* **6901**, Photonic Crystal Materials and Devices VII, 69010K (2008).
14. W. Zhi, R. Guobin, L. Shuqin, J. Shuisheng, *Opt. Exp.* **11**, 980 (2003).
15. J.A. West, C.M. Smith, N.F. Borrelli, D.C. Allan, K.W. Koch, *Opt. Exp.* **12**, 1485 (2004).
16. S.-Jin Im, A. Husakou, J. Herrmann, *Opt. Exp.* **17**, 13050 (2009).
17. F. Tani, J.C. Travers, P.St.J. Russell, *J. Opt. Soc. Am. B* **31**, 311 (2014).
18. M. Bache, Md.S. Habib, C. Markos, J. Lægsgaard, *J. Opt. Soc. Am. B* **36**, 69 (2019).
19. M.H. Frosz, *Opt. Exp.* **17**, 17950 (2009).

Фотонно-кристалічні волокна з трикутною та каґоме структурами для волоконно-оптичних гіроскопів

Є.М. Одаренко, О.С. Гнатенко

Харківський національний університет радіоелектроніки, 61166 Харків, Україна

У статті досліджено фотонно-кристалічні волокна (ФКВ) із трикутною та каґоме структурою для використання у волоконно-оптичних гіроскопах (ВОГ). Обґрунтовано переваги ФКВ для покращення ефективності роботи ВОГ завдяки унікальним характеристикам, таким як висока чутливість, низькі оптичні втрати та стійкість до температурних коливань. Розглянуто механізми локалізації енергії через фотонно-кристалічні заборонені зони та однохвильові режими для збільшення точності вимірювань.Проведено числові розрахунки дисперсійних характеристик та власних мод ФКВ із використанням методу розкладання по плоским хвилям у програмному середовищі MIT Photonic Bands. Проаналізовано модельні властивості різних конструкцій ФКВ, зокрема вплив діаметра порожнистої сердцевини на спектральні характеристики. Показано, що оптимальне співвідношення геометричних параметрів ФКВ забезпечує ефективну локалізацію енергії в порожнистій сердцевині та мінімізацію втрат.Особливу увагу приділено ФКВ із каґоме структурами, що демонструють перспективи для зменшення енергетичних втрат завдяки просторовому розподілу електромагнітного поля. Визначено можливості застосування ФКВ у гіроскопах для авіаційних і оборонних навігаційних систем. Результати дослідження відкривають нові можливості для створення високоточного обладнання, здатного працювати в екстремальних умовах.

Ключові слова: Фотонний кристал, Оптичне волокно, Гіроскоп, Дисперсійні характеристики, Заборонена зона.